Fusion Engineering and Design 85 (2010) 1782–1787

Contents lists available at ScienceDirect

Fusion Engineering and Design

journal homepage: www.elsevier.com/locate/fusengdes

Computer simulation of packing structure in pebble beds

Yixiang Gan[a,b,*], Marc Kamlah[a], Jörg Reimann[a]

[a] Karlsruhe Institute of Technology, D-76344, Eggenstein-Leopoldshafen, Germany
[b] The School of Civil Engineering, The University of Sydney, NSW 2006, Australia

ARTICLE INFO

Article history:
Available online 1 July 2010

Keywords:
Granular materials
Pebble beds
Random close packing
Packing structure
Fusion blankets

ABSTRACT

In HCPB blankets, pebble beds are composed of nearly spherical particles in the state of random closed packing. The packing structure is important to understand responses of pebble beds, e.g., mechanical stresses and effective thermal conductivity. In this paper, an algorithm for random close packing of polydisperse particles is presented which can be used for arbitrary pebble bed containing geometries. The microstructure of a packed bed in both the bulk and near-wall regions can be determined. Computer-generated samples are compared to recent X-ray tomography results of non-compressed pebble beds, including the packing factors and coordination number. Moreover, initial configurations obtained by this method can be used in discrete element simulations of random configurations of pebbles to investigate the overall behaviour of pebble beds under fusion-relevant conditions.

1. Introduction

Pebble beds consist of nearly spherical particles filled into helium-cooled pebble bed (HCPB) blanket systems, as tritium breeder (e.g., Li_4SiO_4 pebbles) and neutron multiplier (beryllium pebbles) materials. The packing structure of these particles is important in blanket applications, since it influences the overall mechanical response [1], the effective thermal conductivity of the bed [2,3], and the interfacial thermal conductance of the pebble–wall interface [4].

From a microscopic point of view, the configuration of particles inside an assembly plays a major role in their overall constitutive behaviour, for instance, different packing factors introduce different mechanical responses to the external excitation [5]. In fusion blankets, the packing factor is one of the key parameters due to the fact that the pebble beds expand during the increase of temperature, and hence thermal stresses are induced. These stresses can change significantly the effective thermal conductivity of the pebble beds. A low packing factor will provide a low effective thermal conductivity, which might be insufficient to conduct the heat generated by neutron irradiation in the pebble bed.

Moreover, gap formation might occur for a loosely packed bed between pebbles and the cooling structure after a few thermal cycles.

The packing factor of a pebble bed depends on different factors: the size and size distribution of pebbles, the dimensions of the blanket, and filling technology [6]. For pebble beds in fusion blankets, the packing factor for mono-sized particles is in the range of 63–64% [7]. To investigate the packing structure and the micromechanics of pebble beds by means of the discrete element method (DEM [8,9,5]), an initial packed configuration should be provided in the range of reasonable packing factors. It is crucial to prepare an initial state of the assembly with both a practical packing factor and topology before the DEM simulation.

The ordered close packing of hard mono-sized spheres has a maximum packing factor of $\eta = \pi/(18)^{1/2} \cong 0.7405$, when the spheres are packed in either the face-centered cubic (FCC) or the hexagonal close-packed (HCP) structure. On the other hand, the packing factor η for experimental packing of mono-sized spheres varies with the method of packing. [10] noted that the experimentally obtainable values of random close packing (RCP) are in the range of 0.64 ± 0.02. The computer simulation of RCP has been studied by various researches [10–14]. Several algorithms have been proposed to get more realistic initial configurations, among which the one suggested by [11] has the advantage to control the final packing factor by a parameter, called the contraction rate κ.

In this paper, we focus on packing issues related to fusion blankets, such as polydisperse packings and packing structures within containers. The algorithm for random close packing of mono-sized particles will be introduced and then extended to polydisperse spherical packing in Section 2. In Section 3, assemblies composed of either mono-sized particles or binary mixtures are generated with the algorithm. In Section 4, comparisons are presented between computed and experimentally determined packing structures [15,16]. Finally, some conclusions will be drawn in Section 5.

* Corresponding author. Tel.: +49 0 7247 823459; fax: +49 0 7247 822347.
E-mail addresses: yixiang.gan@kit.edu, yixiang.gan@sydney.edu.au (Y. Gan).

0920-3796/$ – see front matter © 2010 Elsevier B.V. All rights reserved.
doi:10.1016/j.fusengdes.2010.05.042

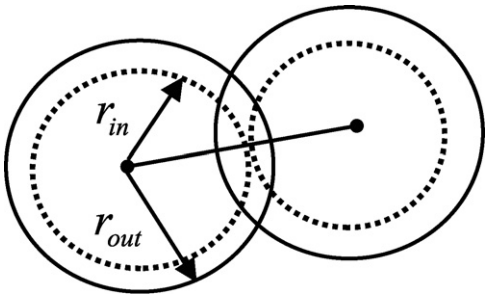

Fig. 1. The definition of r_{out} and r_{in} in a two-particle system.

2. Random close packing algorithm

Jodrey and Tory [11] have proposed an algorithm to obtain RCP of equal-sized spheres by both removing the overlaps and reducing the radius of particles iteratively. First, N spherical particles are generated randomly into a $L \times L \times L$ cube. Initially, the so-called outer radius (r_{out}) of an assembly of N equal-sized particles is set to make the packing factor equal to 1.0, despite the fact that there are overlaps between particles. Meanwhile, a so-called inner radius (r_{in}) is set to be half of the distance between the two closest particles' centers. That means if all particles had a radius of r_{in}, there would be no overlap between particles inside the whole assembly. The definitions of the outer and inner radii are schematically shown in Fig. 1 for the simplest case of two overlapping particles. Each iteration has two functions: first, the worst overlap is removed by moving the two particles away from each other by an equal distance of $r_{out} - r_{in}$, along the line connecting the two centers; second, the outer radius is contracted according to

$$\chi^{(i+1)} = \chi^{(i)} - \frac{(1/2)^j \kappa}{N}, \tag{1}$$

where $\chi^{(i)} = r_{out}^{(i)}/r_{out}^{(0)}$, and $j = \lceil -\log_{10}\Delta\eta^{(i)} \rfloor$. Here, i denotes the number of iterations, N is the number of particles (e.g., $N = 5000$ in this investigation), $\Delta\eta$ is the difference between the packing factors calculated by the outer and inner radii (r_{out} and r_{in}), namely, the nominal packing factor η^n and the true packing factor η^t, respectively. The operator $\lceil \bullet \rfloor$ is the greatest integer function. The parameter κ, which is independent of the size and number of the spheres, characterizes the contraction rate of the assembly. The final configuration is reached, if the condition $r_{out} \le r_{in}$ is satisfied. In an assembly with periodic boundary conditions (PBCs), the parameter κ is the only one to control the contraction rate, and hence different packing factors can be reached by changing κ.

This algorithm was originally based on the idea of concurrently removing the worst overlap and reducing the outer radius, and it can be extended to solve the initial packing problem of polydisperse (multi-sized) particles. To make use of this algorithm in an assembly of polydisperse particles, the outer radius r_{out} and inner radius r_{in} have to be redefined. These radii depend on the size distribution of particles in the assembly. Based on these radii, the method can be specified. Contrary to the mono-sized packing as discussed above, the outer radius and inner radius of each particle may not be identical to the ones of other particles for polydisperse packing.

It is assumed that the distribution of the radii obeys some function $f(I)$ where $1 \le I \le N$ (e.g., $f(I) \equiv 1$ for mono-sized particles). In an assembly of different-sized particles, the radius of each individual particle (e.g., the I-th particle) in the current step, called the outer radius $r_{out}^{(I)}$, can be written as $r_{out}^{(I)} = f(I) \cdot \tilde{r}_{out}$. Here, $\tilde{r}_{out}$ is an outer scaling radius of the assembly.

The value of $\tilde{r}_{out}$ is initially set to yield the nominal packing factor $\eta^n = 100\%$, irrespective of the existence of overlaps in the assembly. For each particle, the corresponding inner radius is $r_{in}^{(I)} = f(I) \cdot \tilde{r}_{in}$. The inner scaling radius $\tilde{r}_{in}$ is chosen in such way that there is no overlap in the assembly. If the distance between two particles I and J is $\delta^{(I,J)}$, then the inner radius of the assembly is defined as

$$\tilde{r}_{in} \equiv \min_{I<J} \left[\frac{\delta^{(I,J)}}{f(I) + f(J)} \right]. \tag{2}$$

The value of $\tilde{r}_{in}$ is determined by searching all overlaps in the target domain as Eq. (2). This pair of particles giving the minimum according to Eq. (2) (for instance, the I-th and J-th particles) is defined as the worst overlap for polydisperse packing. This is reduced to the equal-sized packing case, if $f(I) \equiv 1$. With the size distribution $f(I) \neq 1$, the worst overlap might not equal to the absolute minimum distance, due to the presence of different-sized particles.

Using $\tilde{r}_{out}$ and $\tilde{r}_{in}$, we have the maximum overlap as $\Delta = r_{out}^{(I)} + r_{out}^{(J)} - \delta^{(I,J)}$. To remove this overlap, several different laws can be applied. Here, we propose the general expression of the movement of the I-th particle as

$$d^{(I)} = \Delta \frac{[f(J)]^n}{[f(I)]^n + [f(J)]^n}. \tag{3}$$

Here n can be set to 0, 1, 2 and 3, for equal/linear/square/cubic interpolation, respectively. Equal interpolation means that there is no weight function applied to the movements of the different-sized particles; the cubic interpolation means that the weight function is inverse proportional to the mass of the spherical particles, if they have the same density; n equal to 1 or 2 is something in between. In this investigation, $n = 1$ is used for the sake of simplicity.

According to $\tilde{r}_{in}$ and $\tilde{r}_{out}$, the worst overlap is removed and the outer radii of particles, i.e. $r_{out}^{(I)}$ ($I = 1, 2, ..., N$), are contracted iteratively for polydisperse packing. For each iteration, the nominal and true packing factors are calculated by $\tilde{r}_{out}$ and $\tilde{r}_{in}$, respectively, and the inner radius $\tilde{r}_{in}$ is calculated from the worst overlap by Eq. (2). The worst overlap Δ is removed, the consequence of which is to increase the inner radius $\tilde{r}_{in}$. Then the outer radius $\tilde{r}_{out}$ of the particle assembly is reduced by Eq. (1), while the distribution function $f(I)$ stays unchanged. The iteration will stop and the assembly reaches the finial packing factor, if the difference between $\tilde{r}_{in}$ and $\tilde{r}_{out}$ is smaller than the tolerance.

The evolution of the nominal packing factor η^n and the true packing factor η^t is similar to mono-sized packing.

For polydisperse packing, the radii distribution function $f(I)$ can be varied by several parameters. For instance, a uniform distribution, a normal distribution, etc. can be applied to describe different types of polydisperse packing. The simplest case of polydisperse packing next to the equal-sized packing will be the packing of binary mixtures. The sizes of pebbles vary also in HCPB blankets. For the reference Li_4SiO_4 pebbles, the diameter lies in the range of 0.25–0.63 mm [17].

3. Packing factors for the bulk region

With the implementation of periodic boundary conditions (PBCs), the assemblies represent the bulk region inside pebble beds. Here, we choose mono-sized particles and binary mixtures as examples to demonstrate the RCP algorithm.

3.1. Mono-sized particles

Assemblies with 5000 equal-sized spherical particles have been generated by the RCP algorithm. The contraction rate κ varies from 1×10^{-5} to 1×10^{-3}. For each given contraction rate, several samples have been generated independently.

Fig. 2 shows that we can produce randomly packed assemblies

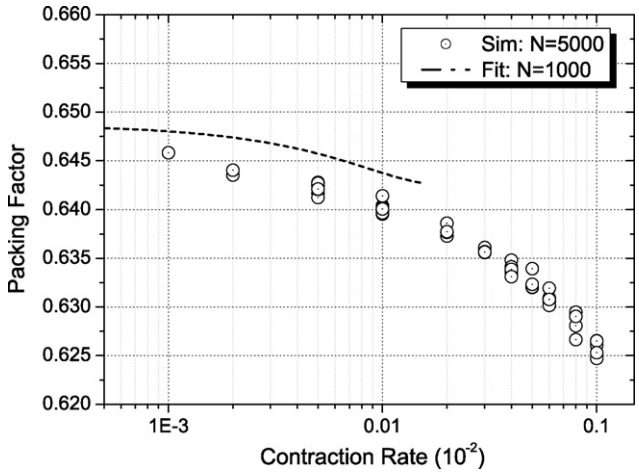

Fig. 2. Variation of packing factor η with the contraction rate κ, $N = 5000$. The dashed line shows the fit for assemblies with 1000 equal-sized particles [11].

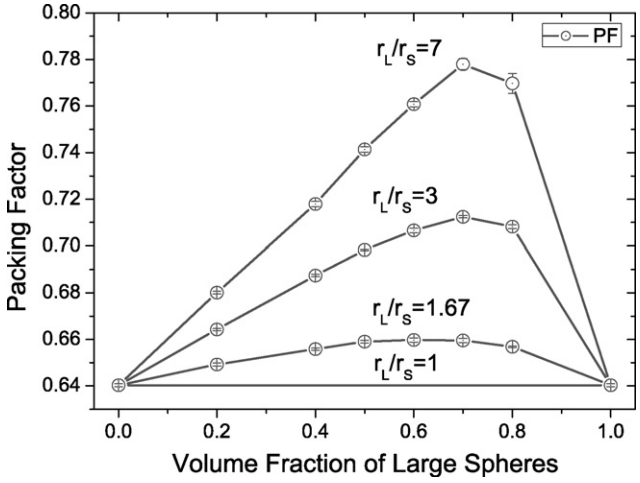

Fig. 3. Packing factors of binary mixtures.

for which $0.625 \leq \eta \leq 0.645$. The packing factor can be controlled roughly by the value of the given contraction rate κ. For the same contraction rate, differences between samples are relatively small. The fitting curve for $N = 1000$ assemblies from [11]. It has to be mentioned that they focused on the region of the dense close packing, is plotted as dashed line for comparison.

3.2. Binary mixtures

One way to increase the packing factor is to fill the spaces between particles with smaller spheres, i.e. to use a binary mixture. There are two parameters to describe the size distribution of particles: the size ratio of large and small particles, r_L/r_S, and the volume fraction of each group of particles, ϕ_L and ϕ_S, where $\phi_L + \phi_S = 1.0$. The relative size and population of the large particles can fully describe the size distribution of the assembly. By varying these two parameters, the packing factor will be changed, and it is interesting to find out the maximum packing factor among different types of binary mixtures used for tuning packing factors inside the blanket. However, large r_L/r_S may introduce size segregation under vibration inside the assembly, and a critical value of $r_L/r_S = 2.78$ has been suggested [18]. In practice, measures have to be taken to avoid segregation effects [19].

First the contraction rate is fixed as $\kappa = 1 \times 10^{-4}$ in this investigation. The changing of the packing factor depending on r_L/r_S and ϕ_L can be found in Fig. 3. Sets of calculations with different size ratios (5/3, 3 and 7) are carried out, and for each data point, 5 samples are made for statistical purposes. For larger size ratios, a higher packing factor η can be obtained for the same volume fraction ϕ_L, while for the same size ratio, the maximum value is reached in the range of volume fraction between 0.7 and 0.8. In literature, the theoretical value of $\phi_L = 0.735$ for the highest packing factor has been suggested [20]. For $r_L/r_S \approx 15$, a value of $\eta \approx 82\%$ was found in experiments [19]. Two obtained assemblies are visualized in Fig. 4(a) $r_L/r_S = 5/3$ and $\phi_L = 0.7$, with a packing factor of $\eta = 0.6606$; (b) $r_L/r_S = 3.0$ and $\phi_L = 0.7$, with $\eta = 0.7123$.

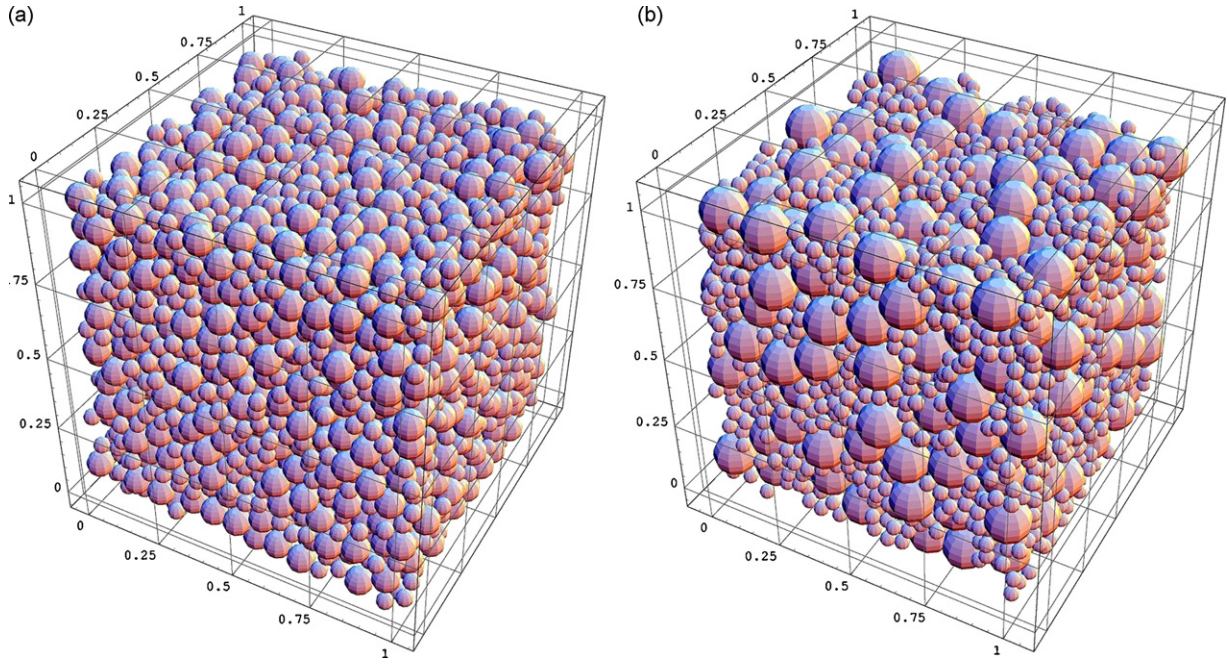

Fig. 4. Visualization of binary mixtures: (a) $r_L/r_S = 5/3$ and $\phi_L = 0.7$; (b) $r_L/r_S = 3.0$ and $\phi_L = 0.7$.

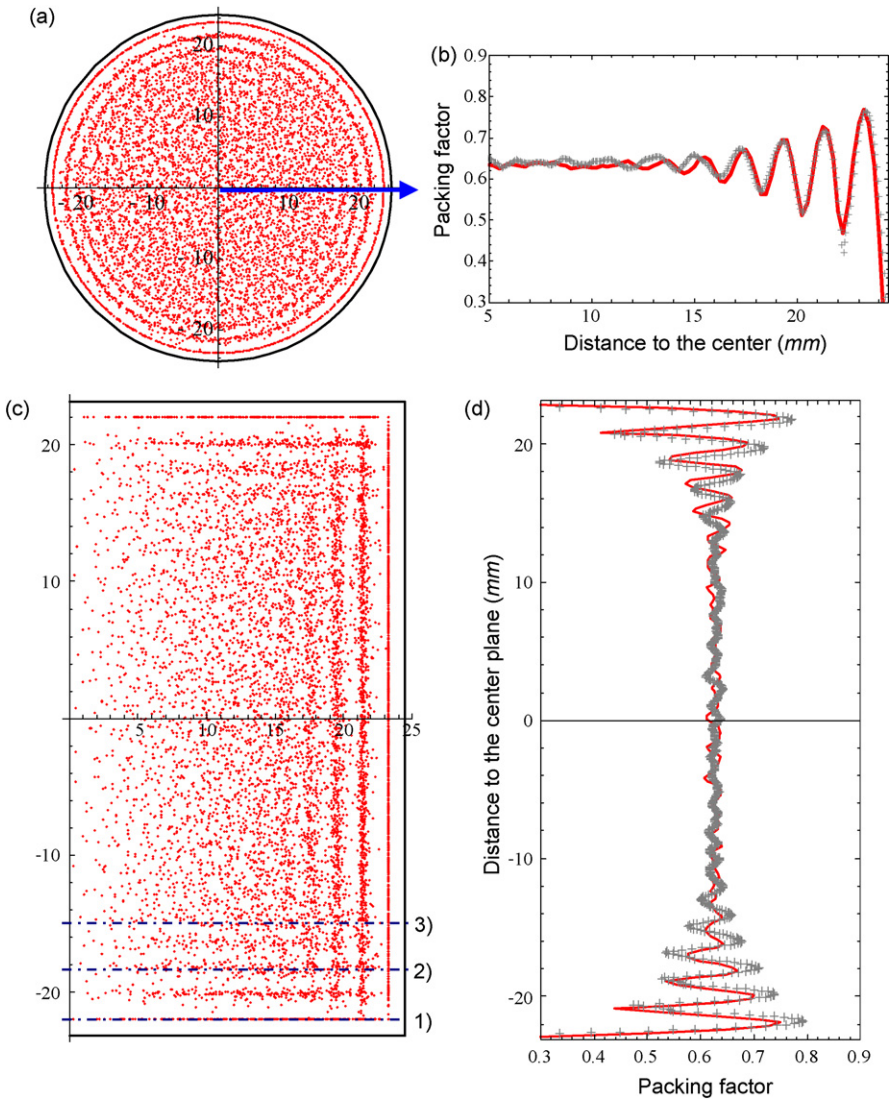

Fig. 5. (a) Radial distribution of particles, particles are projected to the $r-\theta$ plane; (b) packing factor varies over the distance to the wall; (c) vertical distribution of particles, particles are projected to the $r-z$ plane; (d) packing factor varies over the distance to the center plane. The experimental data are shown in (b) and (d) as dots for comparison.

4. Application to pebble beds in cylindrical containers

The pebble arrangements in the vicinity of rigid walls differs characteristically from that in the bulk and results in a different heat transfer behaviour. Detailed high resolution 3D X-ray tomography experiments were performed with aluminium spheres in cylindrical containers in order to determine for both for the bulk and the wall regions the structure of the pebble arrangements, coordination numbers, contact surfaces [15,16]. The sphere packings (sphere diameters $d = 2.3$ mm or 5 mm, inner cylinder diameter $D = 48.9$ mm, height $H \approx 50$ mm) were investigated for a non-compressed or uniaxially compressed state.

In the following, the results from the modified RCP algorithm will be used for comparisons with the results for the non-compressed sphere packing ($d = 2.3$ mm, $H = 46.3$ mm), where a packing factor of $\eta = 61.7\%$ was achieved. The number of particles is calculated by the packing factor and volume, as $N = 3\eta D^2 H/(2d^3) = 8421$.

4.1. Modification to the original code

Concerning the cylinder containers used in X-ray tomography experiments, rigid wall conditions are introduced by the borders of the container. The implementation of rigid wall conditions is realized by monitoring the positions of particles. As long as the particle is overlapping with the rigid wall, the overlap is removed by shifting the particle into the interior of the container. The path of this shifting is in the opposite direction of the surface normal of the container. This is an additional step, and it is independent of removing the worst overlap in the original code with PBCs. The CPU time for generating assemblies in the container does not differ much from the original RCP algorithm discussed previously in the Section 2.

The previous RCP code for N-particle system is dimensionless. The relative value between the particle size and box size is determined by the packing factor, i.e. a denser assembly has a smaller container if the size of particles is fixed. However, in the present case, not only the packing factor η but also the dimensions of the container and particles are fixed and pre-determined. These quantities are related as $\eta = 2Nd^3/(3D^2H)$. To solve this issue, the contraction rate κ is varied to find a packing factor corresponding to the experiment ($\eta = 61.7\%$). Therefore, if the objective packing factor is achieved, the diameter of the particle would be exactly 2.3 mm.

The same principles can be applied to arbitrary pebble bed containers. If an engineering structure is involved, the geometry of the

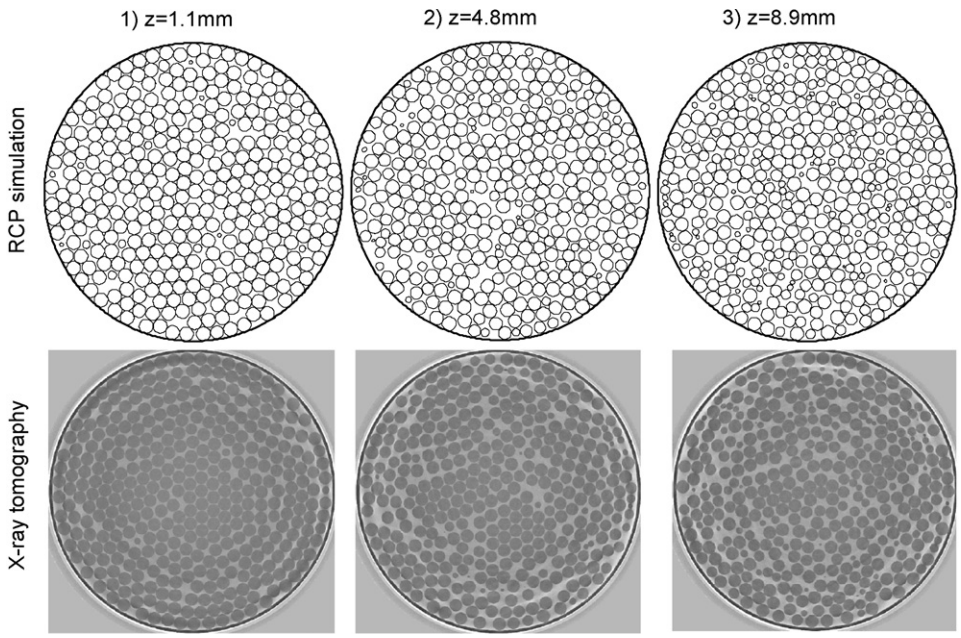

Fig. 6. Cross-sections at $r-\theta$ planes. The first row is the plot from simulation, and the second row is from the experiment [16]. The z-positions of the cross-sections are indicated in Fig. 5(c).

container should be first transferred into the code to identify the interior and exterior regions. If overlaps are found between the container wall and pebbles, the pebbles are shifted into the interior region of the container in the direction of the surface normal.

4.2. Comparison with the experiment

A sample with the packing factor of 61.7% was obtained by setting the contraction rate to $\kappa = 3.5 \times 10^{-4}$. This sample was used in the following for validation.

The calculated particle and packing factor distributions are shown in Fig. 5, with the corresponding experimental results.

First, radial distribution of particles in the $r-\theta$ plane is plotted in Fig. 5(a), with the distribution of corresponding packing factor along r-axis in Fig. 5(b). In Fig. 5(a), there is a transition from regular distribution, in the first few cycles next to the container wall (marked by the solid-black cycle), to random spacial distribution in the interior of the container. In Fig. 5(b), a variation of the packing factor becomes obvious in the region close to the cylindrical wall at a distance of 4–5 particle diameters, as pointed out in literature [15,16,20].

Second, the vertical distribution of particles in the $r-z$ plane is shown in Fig. 5(c). Next to the container wall, there are several regularly packed layers, which have also been observed in the experiment. A corresponding distribution of the packing factor is plotted in Fig. 5(d) as a function of the distance to the center plane. In this case, the regions close to the top and bottom walls have a variation in the packing factor distribution. The corresponding experimental data are shown as dots in Fig. 5(b) and (d) for comparison. The near-wall packing structure differs from the one in the bulk region, which may introduce additional heat transfer resistance to the pebble–wall interface. Since there is no gravity acting on each particles in the simulations, the vertical distribution of packing factor is different from the experiment where asymmetry of the top and bottom regions has been found for un-compressed beds.

Fig. 6 contains results for horizontal cross-sections at distinct vertical distances from the bottom, namely 1.1, 4.8 and 8.9 mm (1st, 3rd and 5th layer from the bottom), respectively, compare Fig. 5(c).

For both the simulation and tomography results, regular hexagonal structures in the inner zone are observed for $z = 1.1$ mm. With increasing distance, a random packing develops. In near-wall regions, the transition from regular to random packing is of major influence on the near-wall heat transfer mechanism which needs to be properly taken into account in the design of fusion blankets.

The original samples generated by the RCP algorithm remove all overlaps in the assembly [11]. That is to say, initially, the coordination number is strictly zero for the assembly.

However, in order to compare to the coordination number in experiments, we set an outer radius, $r^S = (1+\delta)r_0$ (with $\delta = 0.025$ and $r_0 = 1.15$ mm), for searching neighboring particles in contact. If

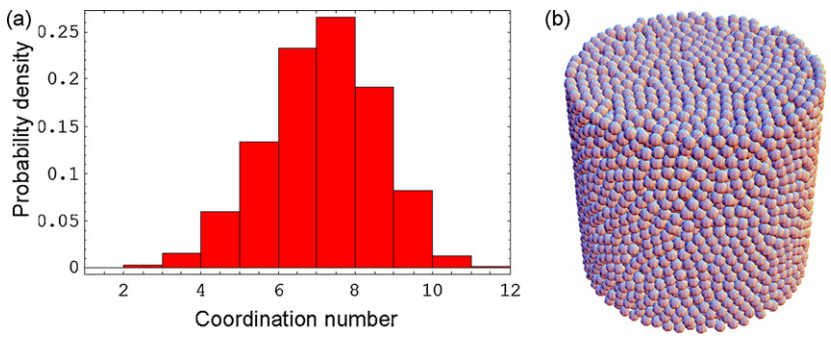

Fig. 7. (a) Probability density of coordination number for internal particles; (b) visualization of the packing structure inside the cylindrical container.

particle J enters this thin shell region between r_0 and r^S of particle I, we define these two particles as contacting particles. Following this assumption, we plot the probability density of coordination number in Fig. 7(a). In this plot, the contacts between the particle and container wall are not taken into account. The coordination number is in the region of $n_C = 2$–12 and a peak exists at $n_C = 7$. This plot has similarities with the experimental data [16], in particular with the compressed samples.

Finally, a visualization of particles inside the container can be found in Fig. 7(b). Near the region of container wall, some regular packing structures can be identified.

5. Conclusion

In this paper, we propose an algorithm for the calculation of the packing structures of pebble beds. Computer simulations using this random close packing algorithm have been applied to assemblies of mono-sized and polydisperse sphere packings. The algorithm can be applied for different types of containers and determines packing structures in the bulk and near-wall zones. The comparison between the simulation and recent X-ray tomography results are shown as a verification of the method. Results, generated by this method, are required to describe the coupled thermal–mechanical behaviour of ceramic breeder blankets.

Acknowledgments

This work, supported by the European Communities under the contract of Association between EURATOM and Forschungszentrum Karlsruhe, was carried out within the framework of the European Fusion Development Agreement. The views and opinions expressed herein do not necessarily reflect those of the European Commission.

References

[1] J. Reimann, D. Ericher, G. Worner, Influence of pebble bed dimensions and filling factor on mechanical pebble bed properties, Fusion Engineering and Design 69 (1–4) (2003) 241–244.
[2] J. Reimann, G. Piazza, H. Harsch, Thermal conductivity of compressed beryllium pebble beds, Fusion Engineering and Design 81 (1–7) (2006) 449–454.
[3] G.J. Cheng, A.B. Yu, P. Zulli, Evaluation of effective thermal conductivity from the structure of a packed bed, Chemical Engineering Science 54 (19) (1999) 4199–4209.
[4] Y.X. Gan, M. Kamlah, Thermo-mechanical modelling of pebble bed–wall interfaces, Fusion Engineering and Design 85 (1) (2010) 24–32.
[5] Y.X. Gan, M. Kamlah, Discrete element modelling of pebble beds: with application to uniaxial compression tests of ceramic breeder pebble beds, Journal of the Mechanics and Physics of Solids 58 (2) (2010) 129–144.
[6] A. Abou-Sena, H. Neuberger, T. Ihli, Experimental investigation on the possible techniques of pebbles packing for the hcpb test blanket module, Fusion Engineering and Design 84 (2–6) (2009) 355–358.
[7] J. Reimann, R. Knitter, G. Piazza, New compilation of the material data base and the material assessment report, Technical report, 2005.
[8] Z. An, A. Ying, M. Abdou, Numerical characterization of thermo-mechanical performance of breeder pebble beds, Journal of Nuclear Materials 367 (2007) 1393–1397.
[9] Z. An, A. Ying, M. Abdou, Application of discrete element method to study mechanical behaviors of ceramic breeder pebble beds, Fusion Engineering and Design 82 (15–24) (2007) 2233–2238.
[10] J.G. Berryman, Random close packing of hard spheres and disks, Physical Review A 27 (2) (1983) 1053.
[11] W.S. Jodrey, E.M. Tory, Computer simulation of close random packing of equal spheres, Physical Review A 32 (4) (1985) 2347–2351.
[12] A.Z. Zinchenko, Algorithm for random close packing of spheres with periodic boundary-conditions, Journal of Computational Physics 114 (2) (1994) 298–307.
[13] S. Torquato, T.M. Truskett, P.G. Debenedetti, Is random close packing of spheres well defined? Physical Review Letters 84 (10) (2000) 2064–2067.
[14] A. Wouterse, A.P. Philipse, Geometrical cluster ensemble analysis of random sphere packings, Journal of Chemical Physics 125 (19) (2006).
[15] J. Reimann, R.A. Pieritz, R. Rolli, Topology of compressed pebble beds, Fusion Engineering and Design 81 (1–7) (2006) 653–658.
[16] J. Reimann, R.A. Pieritz, C. Ferrero, M. Di Michiel, R. Rolli, X-ray tomography investigations on pebble bed structures, Fusion Engineering and Design 83 (7–9) (2008) 1326–1330.
[17] B. Loebbecke, R. Knitter, Procurement and quality control of li4sio4 pebbles for testing of breeder unit mock-ups, Technical report, 2007.
[18] J. Duran, J. Rajchenbach, E. Clement, Arching effect model for particle-size segregation, Physical Review Letters 70 (16) (1993) 2431–2434.
[19] J. Reimann, A. Goraieb, H. Harsch, Thermal conductivity of compressed binary beryllium pebble beds, In Beryllium Workshop-8, Lisbon, Portugal, 2007.
[20] D.J. Cumberland, R.J. Crawford, The Packing of Particles, volume 6 of Handbook of Powder Technology, Elsevier, 1987.